Chemical Engineering Journal 353 (2018) 167–175

Contents lists available at ScienceDirect

Chemical Engineering Journal

journal homepage: www.elsevier.com/locate/cej

Effects of Fe(II) on Cd(II) immobilization by Mn(III)-rich δ-MnO_2

Qian Sun[a,b], Pei-Xin Cui[a], Ting-Ting Fan[a,b,c], Song Wu[a,b], Mengqiang Zhu[d], Marcelo Eduardo Alves[e], Dong-Mei Zhou[a], Yu-Jun Wang[a,*]

[a] Key Laboratory of Soil Environment and Pollution Remediation, Institute of Soil Science, The Chinese Academy of Sciences, Nanjing 210008, China
[b] University of Chinese Academy of Sciences, Beijing 100049, China
[c] Nanjing Institute of Environmental Sciences, Ministry of Environmental Protection of the People's Republic of China, Nanjing 210008, China
[d] Department of Ecosystem Science and Management, University of Wyoming, Laramie, WY 82071, United States
[e] Department of Exact Sciences 'Luiz de Queiroz' Agricultural College – ESALQ/USP, Piracicaba, SP 13418-900, Brazil

HIGHLIGHTS

- Fe(II) decreased Cd(II) retention on Mn(III)-rich δ-MnO_2 at pH 5.5.
- Cd(II) was mainly adsorbed on Mn (III)-rich δ-MnO_2 rather than the newly formed Fe oxides and β-MnOOH.
- Fe(II) addition promoted Cd(II) desorption by altering the surface complexes Cd(II) formed on Mn(III)-rich δ-MnO_2.

GRAPHICAL ABSTRACT

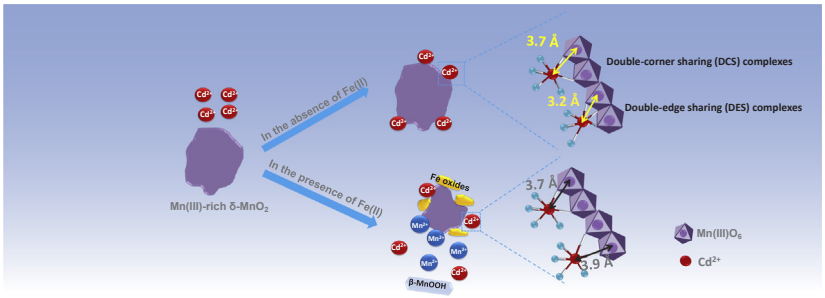

ARTICLE INFO

Keywords:
Mn(III)-rich δ-MnO_2
Cadmium
Ferrous iron
Adsorption
Oxidation
Precipitation

ABSTRACT

Manganese (Mn) oxides have high Cd(II) sorption affinities and could effectively immobilize Cd(II) in soil and aquatic systems. However, coexisting Fe(II) can react with Mn oxides at oxic-suboxic interfaces, thereby affecting Cd(II) immobilization by Mn oxides. Mn(IV)-rich Mn oxides in the environment are readily to be reduced to Mn(III)-rich Mn oxides by natural organic matter. Herein, we determined the effects of Fe(II) on Cd(II) immobilization by Mn(III)-rich δ-MnO_2 (denoted as HE-MnO_2) at pH 5.5 and 7.5. Results show that Fe(II) decreased Cd(II) retention on HE-MnO_2 at pH 5.5 but had no effects at pH 7.5 due to the high Cd(II) adsorption affinity of HE-MnO_2 at high pH. Poorly crystalline Fe oxides, likely ferrihydrite, uniformly precipitated on HE-MnO_2 surfaces upon Fe(II) addition at both pHs. β-MnOOH formed at the high initial Fe(II) concentration at pH 7.5. Cd (II) was mainly adsorbed on HE-MnO_2 rather than the newly formed Fe oxides and β-MnOOH which had low Cd (II) adsorption capacities. The decrease of Cd(II) sorption in the presence of Fe(II) could be explained by the reduction of HE-MnO_2, the precipitation of Fe oxides on HE-MnO_2, and the competition of generated Mn(II) for the sorption sites. Cd(II) formed double-corner sharing (DCS) and double-edge sharing (DES) complexes with Mn (III) edge sites on HE-MnO_2. After the addition of Fe(II), Cd(II) formed only DCS complexes with Mn(III) edge sites. The alternation of the surface complexes caused by Fe(II) promoted Cd(II) desorption from HE-MnO_2. This work suggests that Fe(II) can decrease the removal efficiency of Cd(II) by Mn(III)-rich δ-MnO_2 at oxic-suboxic interfaces in the environment.

* Corresponding author.
E-mail address: yjwang@issas.ac.cn (Y.-J. Wang).

https://doi.org/10.1016/j.cej.2018.07.120
Received 23 May 2018; Received in revised form 7 July 2018; Accepted 17 July 2018
Available online 18 July 2018

1. Introduction

As a nonessential element for human beings, cadmium (Cd) exposure from contaminated soils through food chain and dust would do harm to the liver and kidney, posing great threat to human health [1–3]. Mining wastes and industrial discharge are the main sources of Cd in soils [4–6]. Although the total Cd concentration is low in contaminated soils, the bioavailability of Cd(II) tends to be high because of its weak sorption to common components. However, Mn oxides have high sorption affinity for Cd(II) because of their large amount of negative charges and abundant structural defects [7,8]. Attempts have been made to use Mn oxides to mitigate Cd pollution [1]. Mn oxides effectively reduced Cd solubility and Cd accumulation in wheat [9].

Mn oxides play an important role in controlling the migration and transformation of trace elements and pollutants in the environment [10]. They are strong oxidants and readily reduced by redox-sensitive compounds, such as As(III), Fe(II), Mn(II) and S(II) in the environment [10–12]. The redox reactions can affect metal immobilization by Mn oxides [10,13–15]. Hinkle et al. [15] observed that Mn(II) decreased both Zn(II) and Ni(II) uptake by δ-MnO_2 at pH 4 and that both ions migrated from the interlayer to the edge sites. The effects of Mn(II) on Zn(II) and Ni(II) sorption correlated with Mn(II)-induced structural changes and the competition of Mn(II) for surface sites. Lefkowitz et al. [10] found that Mn(II) led to the desorption of Zn(II) from acid birnessite at pH 6.5, but enhanced Zn(II) sorption at pH 7.5 by the reaction with structural Mn(IV), generating Mn(III) which coprecipitated with Zn(II) and Mn(II) to form Zn-substituted hausmannite.

At oxic-suboxic interfaces in the environment, Fe(II) is a common species and an important reductant for Mn oxides [11,12].

Both Fe(III) and Mn(II) ions, derived from partial reduction of Mn oxides by Fe(II), were adsorbed by Mn oxides [13] or precipitated as ferrihydrite, jacobsite, lepidocrocite and goethite [13,14], depending on the reaction conditions. The sharp reaction between Mn oxides and Fe(II) indicates that Cd(II) immobilization by Mn oxides is likely to be affected by coexisting Fe(II). However, the ternary Fe(II)–Cd(II)–Mn oxides reaction system is essentially unknown and, to our knowledge, unstudied. Most studies focused too much on the sorption behavior of Cd(II) on Mn oxides. A differential pair distribution function (d-PDF) analysis carried out by Genuchten et al. [16] demonstrated that Cd(II) was adsorbed at the vacancy sites of δ-MnO_2. According to the relationship between Mn average oxidation state and Cd(II) sorption behavior, Cd(II) was assumed to be adsorbed at the interlayer of H^+-birnessite [17]. Cd isotopic fractionation was observed in the process of Cd(II) adsorption by H^+-birnessite [18]. Extended X-ray absorption fine structure (EXAFS) spectroscopy showed that Cd(II) was adsorbed to the external surface or migrated into the tunnels in the cryptomelane structure (KMn_8O_{16}) [19]. However, all these studies neglected the impact of Fe(II) on Cd(II) immobilization by Mn oxides. This omission raises important questions directly relevant to the fate of Cd immobilized by Mn oxides in the environments undergoing redox oscillations. In the present study, we thus investigated the effects of Fe(II) on Cd(II) immobilization by Mn oxides. The experiments were conducted at pH 5.5 and 7.5, representing the acidic and slightly alkaline conditions respectively. Higher pH values were not considered in this paper because Cd toxicity is not a serious concern in strongly alkaline environments.

Vernadite, a nanoparticulate layered Mn oxide rich in Mn(IV), is a reactive and abundant Mn oxide in soils and sediments [1,20]. Laboratory studies showed that its synthetic analogue, δ-MnO_2, is readily reduced by natural organic matter (NOM) and as a result, Mn(III) accumulated at the edge and/or vacant sites of δ-MnO_2 [21]. Considering the abundance of NOM, Mn(III)-rich vernadite is probably more common than Mn(IV)-rich vernadite in natural environment. However, despite being easily reduced by NOM in the natural environment, Mn (IV) oxides are often used as the representative Mn oxides in studies dealing with heavy metal immobilization. In this study, Mn(III)-rich δ-MnO_2, prepared by reducing δ-MnO_2 using sodium 4-(2-hydroxyethyl) piperazine-1-ethanesulfonate (HEPES) (denoted as HE-MnO_2), which was more environmentally relevant, was used as the representative Mn oxide, to determine the effects of Fe(II) on Cd(II) immobilization. The reaction products were thoroughly characterized using X-ray powder diffraction (XRD), Fourier transform infrared (FTIR) spectroscopy, X-ray photoelectron spectroscopy (XPS), transmission electron microscopy (TEM), and EXAFS spectroscopy, which could help to disclose, at the molecular scale, the changes in the coordination environments for Cd(II) immobilization by HE-MnO_2 induced by Fe(II). The results provide new insights into the processes governing Cd(II) immobilization by Mn oxides in environments undergoing redox oscillations.

2. Materials and methods

All chemicals used here were of analytical grade or purer. Ultrapure deionized water (> 18 MΩ·cm) was used for preparation of solutions and for rinsing.

2.1. The preparation of HE-MnO_2

HE-MnO_2 was obtained by equilibrating δ-MnO_2 in HEPES buffer. The Mn(III) proportions before and after the treatment were 4.5% and 34% respectively determined using pyrophosphate extraction. The detailed preparation and determination are described in Supplementary Material (SM). It has been reported that δ-MnO_2 generally contained about 14% vacancy sites in the layer, and the HEPES treatment led to 12% of Mn(III) and 2% of Mn(II) occupying the vacancy sites in the form of triple corner-sharing (TCS) complexes above the vacancy sites [22]. The remaining Mn(III) created by the HEPES treatment was located at edge sites instead of the interior of the sheets as supported by the EXAFS and pair distribution function analyses [22]. Our previous study showed that Mn species located at the particle edge sites were all Mn(III), accounting for about 22% of the total Mn [23].

2.2. Cd(II) sorption and desorption on HE-MnO_2 in the absence and presence of Fe(II)

Sorption experiments were carried out in N_2 atmosphere to inhibit Fe(II) oxidation by O_2. 150 mM Fe(II) stock solution and 50 mM Cd(II) stock solution were prepared by dissolving $FeSO_4{\cdot}7H_2O$ or $Cd(NO_3)_2{\cdot}4H_2O$ to deionized water under N_2 atmosphere and stored in the serum bottles. HE-MnO_2 suspension was prepared by dissolving a certain amount of HE-MnO_2 stock suspension in 50 mM $NaNO_3$, which was buffered at pH 5.5 and 7.5 with 50 mM 2-morpholinoethanesulfonic acid (MES) and HEPES respectively and the final Mn concentration was 16.7 mM. Once purged with N_2, the suspensions (30 mL) were transferred to sealed 100-mL serum bottles. Aliquots of Cd(II) and Fe(II) stock solution were added to the HE-MnO_2 suspension, yielding final Cd (II) concentrations at 0, 0.1 and 0.5 mM and Fe(II) concentrations at 0, 0.5 and 5.0 mM. The sample IDs are summarized in Table S1. The suspensions were shaken at 28 °C on a reciprocal shaker. After 76 h, a 1 mL aliquot sampled from the suspension was filtered through a 0.22-μm membrane and added with an equal volume of 1 M HCl for the determination of dissolved Fe, Cd and Mn concentrations. Fe(II) and Fe (III) concentrations were analyzed by UV–vis spectroscopy (UV-2700, Shimadzu, Japan). Dissolved Cd and Mn concentrations were determined using a flame atomic absorption spectrophotometer (Z-2000, Hitachi, Japan).

Desorption experiments were conducted to determine the lability of Cd(II) in the solids. At the end of the sorption experiments, the suspensions were centrifuged, the supernatants were decanted, and the solid phase was resuspended in 30 mL of 50 mM $NaNO_3$ solution buffered at pH 5.5 and 7.5 with 50 mM MES and HEPES, respectively. The suspensions were shaken at 28 °C on a reciprocal shaker. After 42 h, 1 mL aliquots were sampled from the suspensions for the measurement

of dissolved Cd concentrations as described above.

Additional sorption experiments were carried out without the desorption experiment, and the reacted solids were separated from aqueous solutions by centrifugation, rinsed with deionized water, and freeze-dried for the following characterization.

2.3. Characterization of sorption samples

The freeze-dried HE-MnO_2 samples were analyzed by XRD, FTIR, XPS, TEM, and EXAFS spectroscopy. XRD measurements were carried out with a powder diffractometer (Ultima IV, Rigaku, Japan) with Cu Kα radiation. The diffractometer was operated at a tube voltage of 40 kV and a current of 50 mA at a 0.02° 2θ interval using a 25 s counting time per step. For the FTIR analysis, the solid samples were mixed with KBr in an agate mortar for data collection with a Nicolet 5700 spectrometer (Nicolet, USA).

XPS data were collected on an ESCAlLAB-250Xi spectrometer (Theromofisher, Japan) with monochromatic Al Kα radiation (1486.6 eV). Survey and regional scans were collected with a pass energy of 100 eV and 25 eV, and an energy size of 1.0 eV and 0.1 eV, respectively. XPS C1s peaks were used as an inner standard calibration peak at 284.8 eV. XPS peak fitting was performed using a nonlinear least-square fitting program (XPSpeak software 4.1).

The solid samples to be analyzed by TEM were suspended in ethanol and drops of the suspension were deposited onto carbon-coated support film on TEM grids. Spatially resolved elemental maps were acquired using TEM-mapping (JEM-200CX, JEOL, Japan).

For EXAFS spectroscopic analysis, solid samples were pressed into tablets and sealed with Kapton tape for EXAFS data collection. Cd K-edge EXAFS data were collected from selected sorption samples in fluorescence mode and from standard reference samples in transmission mode with Si(3 1 1) monochromator at the beamline BL14W1 of Shanghai Synchrotron Radiation Facility (SSRF). Ag foil was measured concurrently with the samples for internal energy calibration. Data processing was performed using Athena based on IFEFFIT [24]. The k^2-weighted χ(k) function was Fourier transformed using a Hanning window, and all shell-by-shell fitting was conducted in R-space. A single threshold energy value (ΔE_0) was allowed to vary during fitting. A liner combination fitting (LCF) analysis of k^2-weighted EXAFS spectra was used to quantify the proportion of each Cd species in the solids. The reference compounds for the LCF analysis included $Cd(OH)_2$, H^+-birnessite_Cd, γ-MnOOH_Cd, and goethite_Cd. The latter three references were Cd(II)-loaded minerals. The preparation details of these references and the sorption samples are provided in SM.

3. Results and discussion

3.1. Effects of Fe(II) on Cd(II) sorption and desorption by HE-MnO_2

After the sorption, dissolved Fe was detected in none of the reaction systems (data not shown). For the systems with 5.0 mM Fe(II), Fe(II) likely formed large amounts of precipitates because sorption by HE-MnO_2 alone cannot lead to such a high Fe(II) removal. Fe(II) could be oxidized by Mn oxides to generate Fe(III) ions that, in turn, precipitated as Fe(III) oxides when the protons were insufficient [25].

At pH 5.5 in the absence of Fe(II) (pH5.5_0Fe_0.1Cd, pH5.5_0Fe_0.5Cd), ~2.2 mM Mn(II) was released to the solution (Fig. S1), due to the slight reduction by MES buffer, accounting for 15% of the total Mn in HE-MnO_2. A higher amount of Mn(II) (2.4–4.8 mM) was released upon Fe(II) addition, especially in the system with 5.0 mM Fe (II), produced from the reductive dissolution of HE-MnO_2 by Fe(II). However, little Mn(II) was released to the solution at pH 7.5, which was due to the strong adsorption of Mn(II) by Mn oxides and its subsequent oxidation by Mn(IV) in Mn oxides at high pH [21,26].

Cd(II) sorption impacted by Fe(II) is shown in Fig. 1a, b. At pH 5.5, 0.5–5.0 mM Fe(II) reduced the relative Cd(II) uptake from 89.6% to 70.7% when initial Cd(II) concentration was 0.1 mM and from 69.4% to 49.6% when initial Cd(II) concentration was 0.5 mM. Cd(II) was completely removed at pH 7.5 and Fe(II) addition had nearly no effect on the Cd(II) removal, which could be ascribed to the high Cd(II) sorption capacity of HE-MnO_2 at pH 7.5. The addition of 5.0 mM Fe(II) led to no more than 15% dissolution of HE-MnO_2 while Cd(II) sorption at pH 5.5 decreased by 21% and 29% for initial Cd(II) concentration at 0.1 mM and 0.5 mM, respectively, indicating that in addition to the partial dissolution of HE-MnO_2 induced by the Fe(II) addition, other reasons existed for the reduction of Cd(II) sorption. Fe oxides are generally positively charged or electrically neutral at pH 5.5 and 7.5 due to their high isoelectric points (7–9.3) [27,28]. The surface charge of HE-MnO_2 was similar to that of δ-MnO_2 whose isoelectric point was less than 3 [23,29]. Thus, it could be inferred that HE-MnO_2 was negatively charged at pH 5.5 and 7.5. The distinctly different surface charge between HE-MnO_2 and Fe oxides would lead to the different affinities for Cd(II) arising from the electrostatic interactions. It has been reported that Cd(II) sorption on Fe oxides was much lower than that on Mn oxides [8,16]. It was reasonable to speculate that the precipitation of Fe oxides on the surface of HE-MnO_2 was responsible for the reduction of Cd(II) sorption. In contrast, arsenic sequestration by δ-MnO_2 was enhanced in the presence of Fe(II) [30]. That opposite phenomenon was due to the higher As(V) sorption on Fe oxides than that on Mn oxides. In addition, Mn(II) generated from the redox reaction between Fe(II) and HE-MnO_2 might also increase Cd(II) mobility by competition with Cd (II) for sorption sites [15].

Besides inhibiting Cd(II) sorption, the addition of Fe(II) promoted Cd(II) desorption in $NaNO_3$ solution (Fig. 1c, d). At pH 5.5, Fe(II) addition increased Cd(II) desorption from 7.4% to 13.4% when initial Cd (II) concentration was 0.1 mM and from 17.0% to 22.2% when initial Cd(II) concentration was 0.5 mM. It was reasonable to speculate that the binding mechanisms of Cd(II) were altered by Fe precipitation on HE-MnO_2 or the partial reduction of HE-MnO_2, and thus, facilitating Cd (II) desorption. However, Cd(II) desorption at pH 7.5 was less than 1%, even after the addition of Fe(II), demonstrating the strong affinity of HE-MnO_2 for Cd(II) at pH 7.5.

To explain the mechanisms of Cd(II) sorption and desorption on HE-MnO_2 in the presence of Fe(II), further characterizations were conducted.

3.2. XRD and FTIR analyses

The XRD patterns of the reacted solids are shown in Fig. 2. For the systems without Fe(II), the absence of (0 0 1) reflections (24° 2θ) denotes the disorder in the stacking of the phyllomanganate sheets along the c-axis, and those at 37° and 66° 2θ suggest hexagonal layer symmetry [31]. The low intensities of the diffraction peaks are consistent with small particle sizes of δ-MnO_2. For the systems with Fe(II), obvious changes occurred to XRD patterns of pH7.5_5.0Fe_0.5Cd, where the characteristic peaks of feitknechtite (β-MnOOH) (19.2°, 33.3°, 35.2°, 37.7°, 44.0°, 49.3°, 58.5° 2θ) appeared. These peaks are not observed in other systems, indicating that high pH and high Fe(II) concentrations favored β-MnOOH formation. Formation of β-MnOOH was also observed during the reduction of δ-MnO_2 by fulvic acid, Fe(II) and HS^- in previous studies [21,32]. Lefkowitz et al. [26] reported that β-MnOOH was produced when acid birnessite reacted with Mn(II) at pH 7.0–8.5 while no mineralogical transformation occurred at pH < 7, consistent with our results that β-MnOOH was only found in samples reacted at pH 7.5 but not at pH 5.5.

No characteristic peaks of Fe oxides are observed in the XRD patterns, suggesting the formation of poorly crystallized Fe oxides, likely ferrihydrite, which is hard to detect by XRD [33].

FTIR spectra of samples are shown in Fig. 3. The peak at 760 cm^{-1} arose from the vibration of Mn-O [34]. This peak disappeared with the addition of 5.0 mM Fe(II), suggesting that HE-MnO_2 was severely corroded by high Fe(II) concentrations. New peaks emerged at 946 cm^{-1}

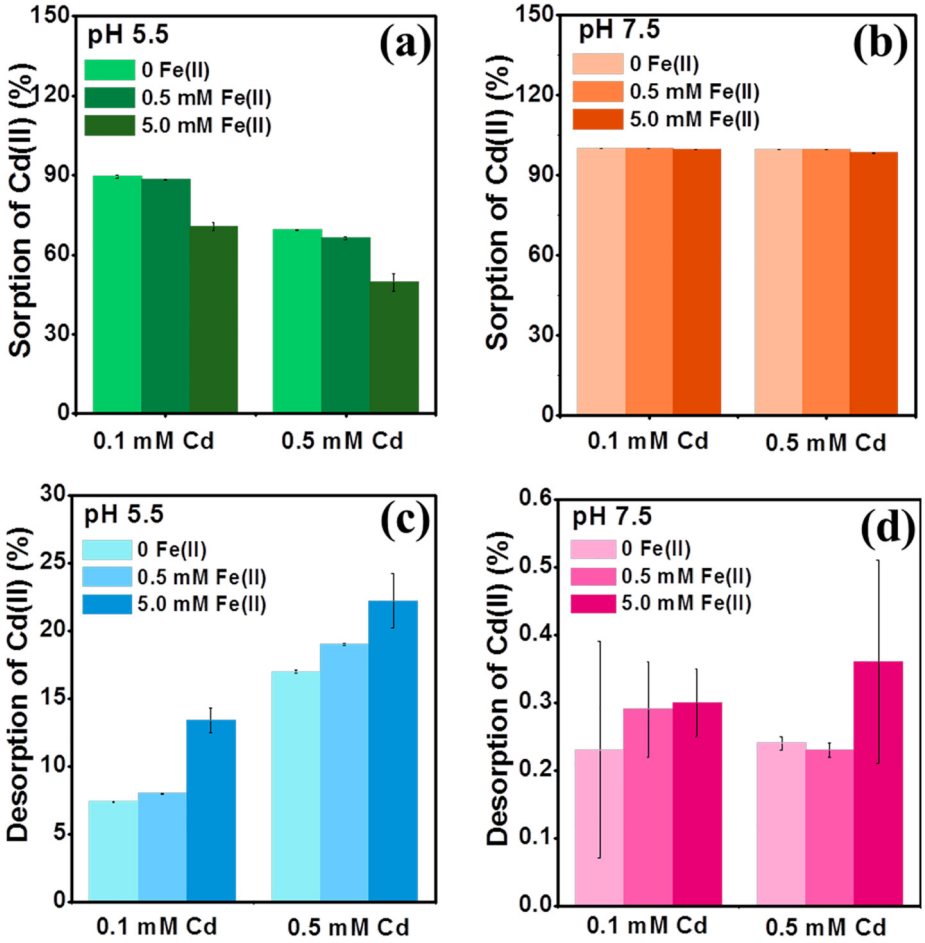

Fig. 1. Effects of Fe(II) on Cd(II) sorption and desorption by HE-MnO_2.

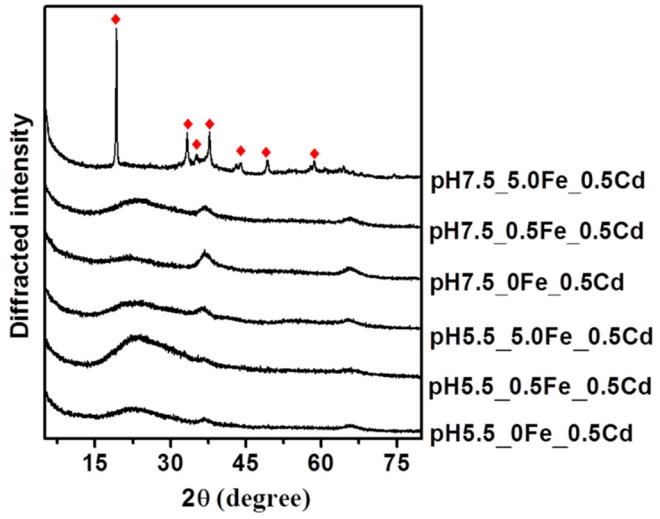

Fig. 2. XRD patterns for samples and the red diamonds denote the reflection diffraction of β-MnOOH.

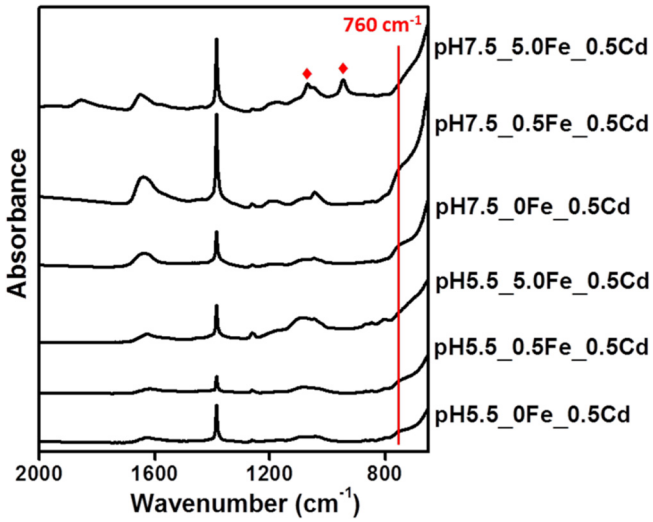

Fig. 3. FTIR spectra for samples and the red diamonds denote the peaks of β-MnOOH.

and 1067 cm^{-1} in pH7.5_5.0Fe_0.5Cd, which are the characteristic peaks of β-MnOOH [35], in line with the XRD results.

3.3. X-ray photoelectron spectroscopy

The theoretical molar ratios of Fe to Mn in the bulk phase (added Fe (II)/(total Mn – dissolved Mn(II)) and the molar ratios determined from XPS survey spectra (Fig. S2a) for the reacted samples are shown in Table S2. Because the elemental data provided by XPS mainly reflects the composition of solid surfaces, the higher Fe / Mn ratio determined by XPS than that in the bulk phase indicated that Fe was enriched, i.e., precipitated on the surface of HE-MnO_2, covering the signal of Mn. High-resolution XPS spectra of Fe2p are shown in Fig. S2b. Binding energy (BE) of $Fe2p_{3/2}$ for all samples were ~711 eV. It is difficult to

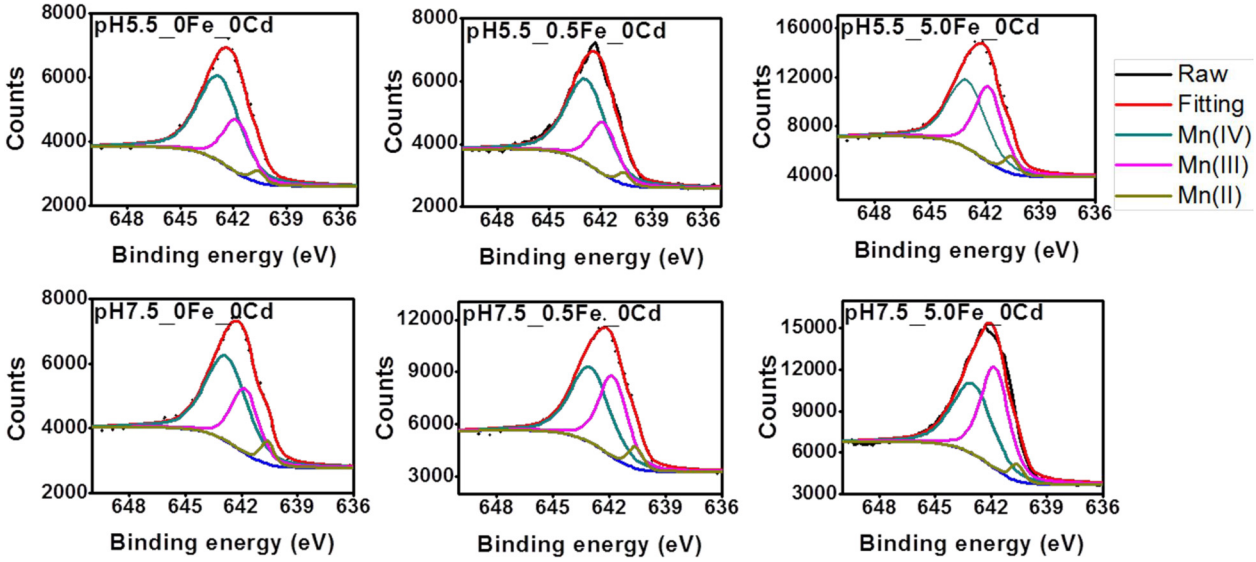

Fig. 4. XPS results of Mn2p spectra of samples and their corresponding fitting curves are also given.

estimate the Fe valence through the binding energy of $Fe2p_{3/2}$ because of the overlapping of the binding energy of Fe(II) and Fe(III) compounds, which varies from 706.5 to 711.0 and 710.2 to 713.3 eV, respectively [34]. It was reported that the $Fe2p_{3/2}$ satellite peaks of Fe(II) and Fe(III) were around 715 eV and 719 eV respectively while the $Fe2p_{1/2}$ satellite peaks of Fe(II) and Fe(III) were around 729.0 eV and 732.5 eV respectively [36]. The large difference between Fe2p satellite peaks of Fe(II) and Fe(III) could favor the discrimination of the two Fe valences in samples. $Fe2p_{3/2}$ satellite peak located at 719 eV, and Fe2p1/2 satellite peak located at 732 eV in both pH5.5_5.0Fe_0Cd and pH7.5_5.0Fe_0Cd, indicating that the oxidation state of Fe in these samples were all Fe(III), i.e., all Fe(II) added to the system was oxidized to Fe(III) by HE-MnO_2. Although the weak peaks of Fe in pH5.5_0.5Fe_0Cd and pH7.5_0.5Fe_0Cd hindered the estimation of the Fe valence, it could be speculated that Fe in pH5.5_0.5Fe_0Cd and pH7.5_0.5Fe_0Cd was also Fe(III) because of the lower amounts of Fe(II) added.

High-resolution XPS spectra of $Mn2p_{3/2}$ and corresponding peak fitting results are shown in Fig. 4 and Table S3. The fitted $Mn2p_{3/2}$ peak position for Mn(II) ranged from 640.8 to 641.0 eV, the Mn(III) peak ranged from 641.8 to 642.0 eV, and Mn(IV) ranged from 642.6 to 643.0 eV, consistent with previous studies [37]. The molar ratio of Mn (II):Mn(III):Mn(IV) in HE-MnO_2 without the addition of Fe(II) was about 2:24:74, rather close to the results acquired by pyrophosphate extraction method and those reported by Simanova et al. [22]. After reacting with 0.5 mM Fe(II), the average oxidation state of HE-MnO_2 slightly decreased from 3.72 to 3.68 at pH 5.5 and from 3.71 to 3.65 at pH 7.5 (Table S3), due to the slight reduction of HE-MnO_2 by Fe(II). In the systems where 5.0 mM Fe(II) was added, the proportion of Mn(IV) decreased from 74% to 49%, accompanied with the increase of the Mn (II) and Mn(III) proportions, leading to the large reduction of the average oxide oxidation states (AOS) of HE-MnO_2, consistent with Fe2p XPS results that all Fe(II) was oxidized to Fe(III).

3.4. Transmission electron microscopy

pH5.5_0Fe_0Cd, pH5.5_5.0Fe_0.5Cd and pH7.5_5.0Fe_0.5Cd were characterized using TEM (Fig. 5). In the systems without Fe(II) and Cd (II), the particle sizes of HE-MnO_2 were about 20 nm (Fig. 5a). The flocculated morphology and the selected-area electron diffraction (SAED) pattern indicated poor crystallinity of HE-MnO_2, consistent with the XRD data. After reacting with 5.0 mM Fe(II) at pH 5.5 and 7.5, the morphology of the mineral phase was no longer flocculated (Fig. 5b, c), likely arising from the precipitation of Fe oxides on HE-MnO_2. The molar ratio of Mn:Fe:Cd was 69.3:24.1:6.6 in area I for pH5.5_5.0Fe_0.5Cd, close to the theoretical value in this sample. New phases with the diameter of ~200 nm were observed in area II for pH7.5_5.0Fe_0.5Cd. The SAED pattern of area II indicated the high degree of crystallinity of the new phases. The molar ratio of Mn:Fe:Cd in this area was 95.6:3.3:1.1, suggesting its enrichment of Mn. Considering the FTIR and XRD results, the bulk materials in area II were likely to be β-MnOOH. The ratio of Cd:Mn in area II was significantly lower than that in area I, demonstrating that the Cd(II) sorption capacity on β-MnOOH was much lower than that on HE-MnO_2, which might be due to the high isoelectric point of β-MnOOH at pH 7.5 and its high degree of crystallinity.

EDS (energy dispersive X-ray spectroscopy) mapping of selected areas in pH5.5_5.0Fe_0.5Cd and pH7.5_5.0Fe_0.5Cd are shown in Fig. S3. The distribution of Fe and Mn are similar, suggesting that Fe precipitated uniformly on the surface of Mn oxides at pH 5.5 and 7.5 rather than forming Fe oxides separated from Mn oxides. Cd distribution completely overlapped with Fe and Mn distribution, demonstrating that Cd(II) was adsorbed uniformly by the Fe-Mn oxides. However, it was hard to verify whether Cd(II) was mainly adsorbed by Mn oxides or newly formed Fe oxides, which could be revealed by EXAFS spectroscopy.

3.5. EXAFS spectroscopy

To investigate the microscopic mechanisms of Cd(II) sorption on HE-MnO_2 in the presence of Fe(II), Cd K-edge EXAFS spectra for sorption samples were collected, which were analyzed by LCF and shell-by-shell fitting. According to the LCF analysis (Fig. 6, Table 1), the proportion of $Cd(OH)_2$ was 19–37% in all samples, indicating that a portion of Cd(II) formed as $Cd_x(OH)_y$ polymers on HE-MnO_2. $Cd_x(OH)_y$ polynuclear complexes were also found to form when Cd(II) was adsorbed by kaolinite and red mud using EXAFS spectroscopy [38,39]. The polynuclear complexes were formed due to the accumulation of adsorbed Cd(II). In the systems with Fe(II) added, a negligible proportion of Cd(II) (0–7%) existed as goethite_Cd, indicating that Cd(II) was mainly adsorbed by Mn oxides even in the presence of Fe oxides, arising from the much higher Cd(II) sorption capacity of Mn oxides than Fe oxides. H^+-birnessite was rich in vacancies [40], and Cd(II) was adsorbed mainly on those vacancies [16,19]. The absence of H^+-birnessite_Cd in the LCF analysis for all samples indicated that Cd(II) was not adsorbed on vacancies but at the edge sites of HE-MnO_2. This is

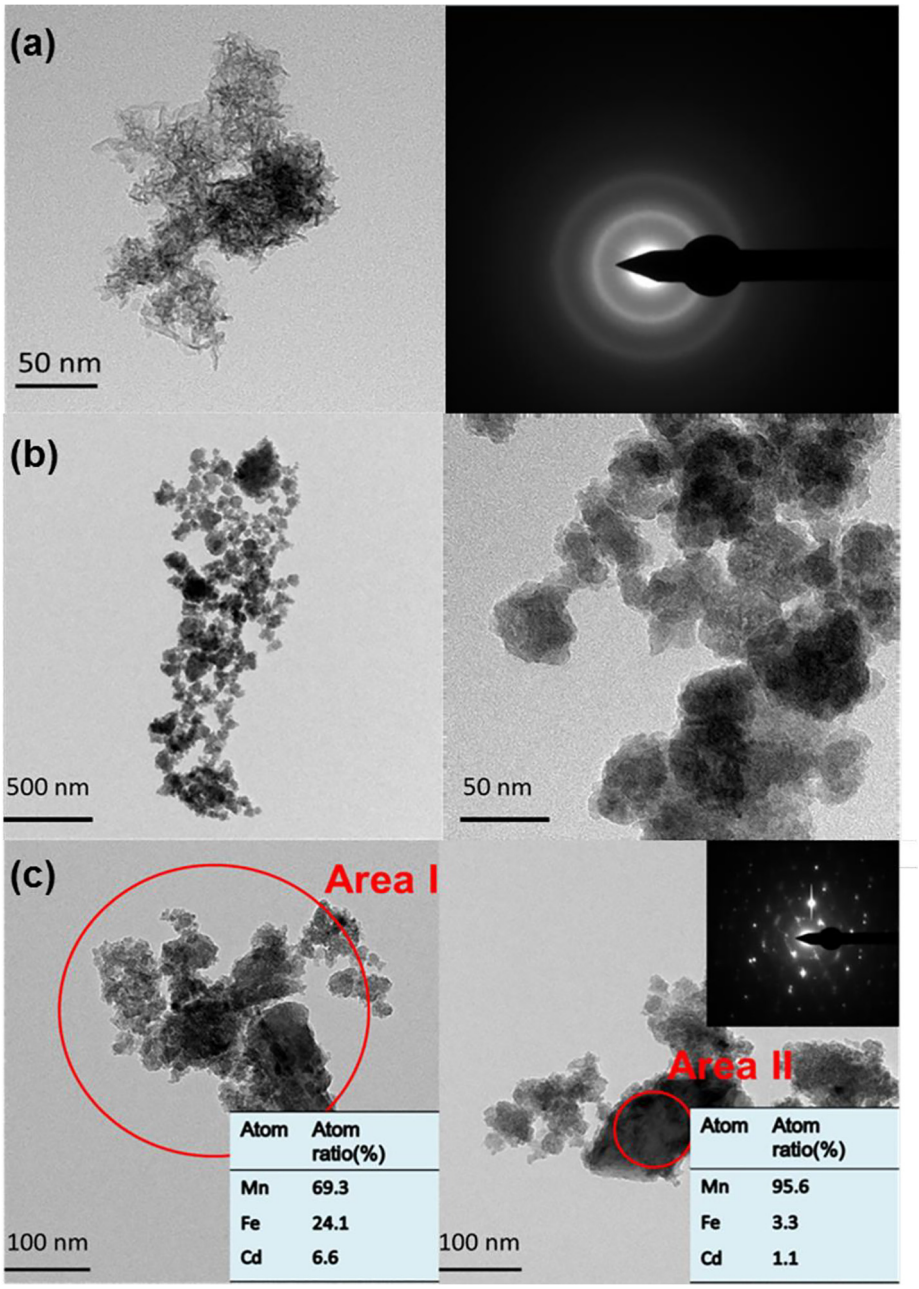

Fig. 5. TEM images of (a) pH5.5_0Fe_0Cd, (b) pH5.5_5.0Fe_0.5Cd and (c) pH7.5_5.0Fe_0.5Cd.

because that the presence of abundant Mn(III) in HE-MnO_2 blocked the vacancies for Cd(II) adsorption due to the high affinity of Mn(III) to vacancies of Mn oxides [21], and thus, edge sites became important and the major sites for Cd(II) adsorption. It was reported that Ni was mainly sorbed at the vacancy sites of δ-MnO_2 while most Ni was sorbed at the edge sites in Mn(III)-rich δ-MnO_2 [22]. In contrast, the contribution of γ-MnOOH_Cd was significant (63–77%) for all samples. Considering that all Mn is Mn(III) in γ-MnOOH, it was reasonable to speculate that Cd(II) was mainly bound with Mn(III) sites, consistent with the fact that Mn species located at the particle edge of HE-MnO_2 were all Mn(III).

Shell-by-shell fitting results are shown in Fig. 7 and Table 2. In all samples the coordination numbers of Cd-O shell were close to 6 and the Cd-O distances were ~2.3 Å, indicating that the adsorbed Cd(II) was in an octahedral environment [41]. The Cd-Fe path was not considered in the process of shell fitting because of the little contribution of Fe oxides to Cd(II) adsorption implicated by the LCF analysis. Only the second shell of Cd-Mn was fitted. The fitting returned two Cd-Mn shells with the distances of 3.72–3.76 Å and ~3.2 Å in the absence of Fe(II).

Generally, the metal-Mn distance depends on the coordination structure metal ions forming with MnO_6 [41], Mn valence in MnO_6 [22], and the protonation of the surface O to which metal binds [42]. When distorted MnO_6 and CdO_6 polyhedra linked as a face sharing complex, the Cd-Mn distance was shorter than 3 Å. When an edge sharing complex was formed, the Cd-Mn distance ranged from 3.0 to 3.4 Å. When a double corner sharing (DCS) complex was formed, the Cd-Mn distance ranged from 3.6 to 4.2 Å [41]. The Ni-Mn distance was 0.18 Å larger when Ni formed an edge-sharing complex on HE-MnO_2 than δ-MnO_2 owing to the larger radius of Mn(III) than Mn(IV) [22]. For the double edge sharing (DES) complex Pb(II) formed on hexagonal birnessite, the Pb-Mn distance increased by 0.11–0.22 Å when O in MnO_6 correlating with PbO_6 was protonated [42]. Several investigations have reported the Cd-Mn distance when Cd(II) was adsorbed by Mn oxides. Bochatay et al. [41] investigated Cd(II) sorption complexation on γ-MnOOH using EXAFS spectroscopy and found that the

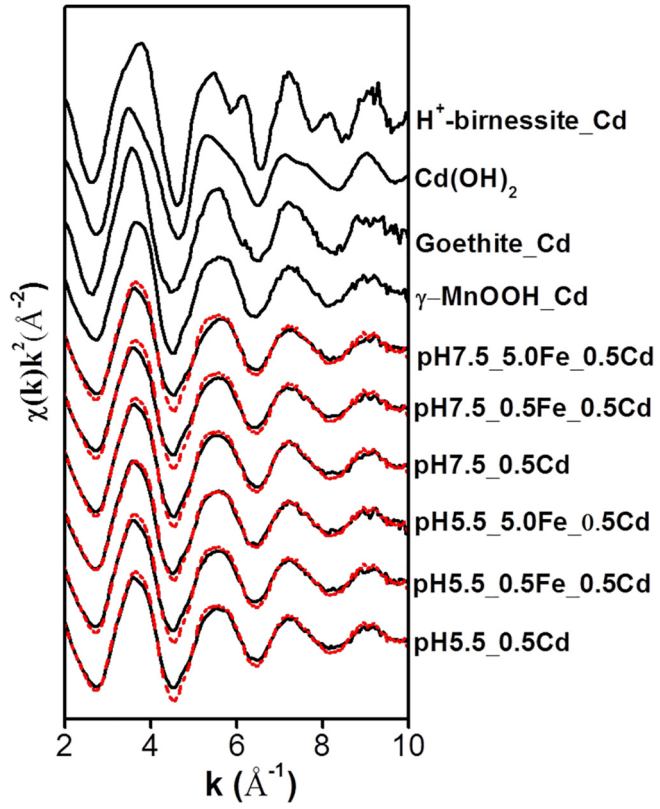

Fig. 6. Cd k^2-weighted EXAFS spectra for Cd reference standard and Cd(II) sorption samples (solid curves), overlapped with LCF results (scatter curves).

Table 1
Results of LCF analysis of the Cd K-edge EXAFS spectra for samples reacted under various conditions.

Sample ID	Proportion (%)			R-factor
	γ-MnOOH_Cd	Goethite_Cd	$Cd(OH)_2$	
pH5.5_0.5Cd	64	0	36	0.033
pH5.5_0.5Fe_0.5Cd	73	3	24	0.039
pH5.5_5.0Fe_0.5Cd	74	7	19	0.033
pH7.5_0.5Cd	73	0	27	0.027
pH7.5_0.5Fe_0.5Cd	77	2	21	0.055
pH7.5_5.0Fe_0.5Cd	65	0	35	0.058

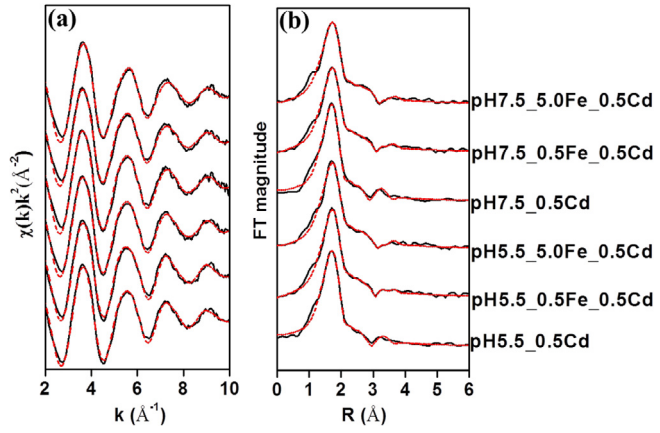

Fig. 7. (a) Cd K-edge EXAFS spectra and (b) and the Fourier transforms for Cd reference standard and Cd(II) sorption samples (solid curves), overlapped with shell fitting results (scatter curves).

distance was 3.2 Å and they attributed this distance to the edge sharing complexes Cd(II) formed with $Mn(III)O_6$. Randall et al. [17] investigated Cd(II) sorption on cryptomelane, which has a tunneled structure using EXAFS spectroscopy, and found that the Cd-Mn distance was 3.65 Å with Mn coordination number at 4.9, demonstrating that Cd (II) formed corner sharing complexes with MnO_6. The Cd-Mn distance for Cd(II) sorption by δ-MnO_2 was 3.66 Å deduced from differential pair distribution function results, which arose from the TCS complexes of Cd (II) formed at the vacancy sites of δ-MnO_2 [16]. Our unpublished data also showed that the Cd-Mn distance was 3.66 Å and Cd-Mn coordination number was close to 6, when Cd(II) was adsorbed on δ-MnO_2, arising from Cd(II) occupation at the vacancy sites. The Cd-Mn distance of 3.72–3.76 Å in the present study was slightly longer than those found in TCS complexes (3.66 Å), and the corresponding coordination numbers were small (1.6–1.8), demonstrating that Cd(II) formed DCS complexes at the edge sites of HE-MnO_2, in agreement with LCF results. The elongation of Cd-Mn distance was likely due to Cd(II) binding with $Mn(III)O_6$ considering that only Mn(III) sites were located at the edge of HE-MnO_2. The distance of 3.2 Å could be attributed to the DES complexes to Mn(III) edge sites.

In the systems with Fe(II) added, two Cd-Mn distances of 3.7 Å and 3.9 Å were returned. The Cd-Mn distances were 3.47 Å and 3.97 Å in the structure of $CdMn_2O_4$, where 3.97 Å arose from the DCS complexes of CdO_6 with $Mn(III)O_6$. Thus, the surface complexes of Cd(II) formed with HE-MnO_2 transformed from DES and DCS complexes to only DCS complexes upon Fe(II) addition, which might be due to that Fe oxides formed on the surface of HE-MnO_2 or the partial reduction of HE-MnO_2 altered available surface sites of HE-MnO_2 for Cd(II). The alternation of Cd(II) coordination associated with HE-MnO_2 after Fe(II) addition could well interpret the higher Cd(II) desorption with Fe(II) addition. It could be inferred that DCS complexes of Cd(II) formed on HE-MnO_2 had a lower binding energy than DES complexes, and thus, easy to be desorbed. Edge-sharing complexes were generally thought to be more stable than corner-sharing complexes [43]. Previous DFT results showed that DCS complexes Pb(II) formed on the edge sites of hexagonal birnessite were less stable than DES complexes [42].

4. Conclusions

Reaction of Fe(II) with HE-MnO_2 led to the formation of poorly crystalline Fe oxides, likely ferrihydrite, precipitated uniformly on the surface of HE-MnO_2, the partial dissolution of HE-MnO_2, and reduction of the average Mn valence in HE-MnO_2. Well crystallized β-MnOOH was generated at pH 7.5 with a high Fe(II) concentration. The addition of Fe(II) reduced Cd(II) immobilization on HE-MnO_2 at pH 5.5 whereas had nearly no effect on Cd(II) immobilization at pH 7.5 because of the extremely high affinity of HE-MnO_2 for Cd(II). Cd(II) was adsorbed on HE-MnO_2 rather than newly formed Fe oxides and β-MnOOH, which have lower affinities for Cd(II) than HE-MnO_2. Thus, the decrease of Cd (II) sorption in the presence of Fe(II) was mainly due to the reduction of HE-MnO_2, the precipitation of Fe oxides on HE-MnO_2 and the competition of generated Mn(II) for the sorption sites. Adsorbed Cd(II) formed DES and DCS complexes with Mn(III) edge sites on HE-MnO_2. After the addition of Fe(II), Cd(II) only formed DCS complexes on HE-MnO_2, which might be due to that the partial reduction of HE-MnO_2 or Fe oxides precipitated on HE-MnO_2 changed the available surface sites for Cd(II). Cd(II) desorption was enhanced in the presence of Fe(II), especially at pH 5.5, which could be explained by the lower binding energy of DCS complexes Cd(II) formed on HE-MnO_2 than DES complexes.

Our findings shed light on the Cd(II) immobilization by Mn oxides in environments where Fe(II) coexists with Mn oxides at the oxic-suboxic interface. The presence of Fe(II) would reduce the removal and increase the mobility of Cd(II) under acidic conditions. Mn oxides have an extremely high sorption capacity for Cd(II) as shown in this study. It is therefore reasonable to assume that a small amount of Mn oxides is sufficient for effective immobilization of Cd(II) in the soil. Mn oxides

Table 2
Results of shell-by-shell fitting of the Cd K-edge EXAFS spectra for samples reacted under various conditions.

Sample ID	ΔE_0 (eV)	Shell	Coordination number	R (Å)	σ^2 (Å^2)	R-factor
pH5.5_0.5Cd	5.6 ± 0.5	Cd-O	5.5 ± 0.2	2.27 ± 0.01	0.0111	0.0021
		Cd-Mn	1.6 ± 0.7	3.76 ± 0.04	0.0167	
		Cd-Mn	0.5 ± 0.4	3.21 ± 0.07	0.0167	
pH5.5_0.5Fe_0.5Cd	4.5 ± 0.5	Cd-O	5.8 ± 0.3	2.27 ± 0.01	0.0120	0.0017
		Cd-Mn	2.2 ± 1.5	3.69 ± 0.03	0.0128	
		Cd-Mn	1.7 ± 1.0	3.89 ± 0.05	0.0128	
pH5.5_5.0Fe_0.5Cd	4.2 ± 0.5	Cd-O	6.1 ± 0.3	2.26 ± 0.01	0.0122	0.0026
		Cd-Mn	1.9 ± 0.7	3.68 ± 0.04	0.0128	
		Cd-Mn	1.8 ± 0.8	3.87 ± 0.05	0.0128	
pH7.5_0.5Cd	5.2 ± 0.5	Cd-O	5.4 ± 0.2	2.27 ± 0.01	0.0105	0.0021
		Cd-Mn	1.8 ± 0.6	3.72 ± 0.03	0.0151	
		Cd-Mn	0.4 ± 0.4	3.20 ± 0.08	0.0151	
pH7.5_0.5Fe_0.5Cd	4.7 ± 0.5	Cd-O	5.6 ± 0.3	2.27 ± 0.01	0.0121	0.0017
		Cd-Mn	2.2 ± 1.4	3.70 ± 0.03	0.0132	
		Cd-Mn	2.1 ± 1.1	3.89 ± 0.04	0.0132	
pH7.5_5.0Fe_0.5Cd	4.8 ± 0.5	Cd-O	5.8 ± 0.3	2.26 ± 0.01	0.0122	0.0026
		Cd-Mn	2.4 ± 0.7	3.71 ± 0.03	0.0132	
		Cd-Mn	2.1 ± 0.8	3.90 ± 0.04	0.0132	

could be widely used in Cd-contaminated soils, excepting for the acidic ones, which are prone to flooding where Fe(II) coexists with Mn oxides and would inhibit Cd(II) immobilization by Mn oxides. Further studies are required to explore effects of other coexisting compounds such as Mn(II) and organic matter on Cd(II) immobilization by Mn oxides.

Acknowledgements

This study was supported by the National Key Research and Development Program of China (2016YFD0800407), and the National Natural Science Foundation of China (projects No. 41771276 and 41422105). We acknowledge Shanghai Synchrotron Radiation Facility BL14W for EXAFS beam time. M.Z. acknowledges the support from the U.S. Department of Energy Experimental Program to Stimulate Competitive Research Office for financial support (DOE-EPSCoR DE-SC0016272).

Appendix A. Supplementary data

The preparation of HE-MnO_2 and the determination of Mn(III), the preparation of samples for EXAFS analysis, Tables S1–3, and Figs. S1–3. Supplementary data to this article can be found online at https://doi.org/10.1016/j.cej.2018.07.120.

References

[1] A. Suda, T. Makino, Functional effects of manganese and iron oxides on the dynamics of trace elements in soils with a special focus on arsenic and cadmium: a review, Geoderma 270 (2016) 68–75.
[2] T. Schütz, S. Dolinská, P. Hudec, A. Mockovčiaková, I. Znamenáčková, Cadmium adsorption on manganese modified bentonite and bentonite–quartz sand blend, Int. J. Miner. Process. 150 (2016) 32–38.
[3] D. Mohan, C.U.P. Jr, P.H. Steele, Single, binary and multi-component adsorption of copper and cadmium from aqueous solutions on Kraft lignin-a biosorbent, J. Colloid Interface Sci. 297 (2006) 489–504.
[4] C.H. Lai, C.Y. Chen, B.L. Wei, S.H. Yeh, Cadmium adsorption on goethite-coated sand in the presence of humic acid, Water Res. 36 (2002) 4943–4950.
[5] K.A. Barrett, M.B. Mcbride, Dissolution of zinc-cadmium sulfide solid solutions in aerated aqueous suspension, Soil Sci. Soc. Am. J. 71 (2007) 322–328.
[6] A. Voegelin, R. Kretzschmar, Modelling sorption and mobility of cadmium and zinc in soils with scaled exchange coefficients, Eur. J. Soil Sci. 54 (2003) 387–400.
[7] M. Villalobos, B. Toner, J. Bargar, G. Sposito, Characterization of the manganese oxide produced by Pseudomonas putida strain MnB1, Geochim. Cosmochim. Acta 67 (2003) 2649–2662.
[8] A. Turner, S.M.L. Roux, G.E. Millward, Adsorption of cadmium to iron and manganese oxides during estuarine mixing, Mar. Chem. 108 (2008) 77–84.
[9] Z.S. Chen, G.J. Lee, J.C. Liu, The effects of chemical remediation treatments on the extractability and speciation of cadmium and lead in contaminated soils, Chemosphere 41 (2000) 235–242.
[10] J.P. Lefkowitz, E.J. Elzinga, Impacts of aqueous Mn(II) on the sorption of Zn(II) by hexagonal birnessite, Environ. Sci. Technol. 49 (2015) 4886–4893.
[11] X. Han, Y.L. Li, J.D. Gu, Oxidation of As(III) by MnO_2 in the absence and presence of Fe(II) under acidic conditions, Geochim. Cosmochim. Acta 75 (2011) 368–379.
[12] M. Siebecker, A.S. Madison, G.W. Luther, Reduction kinetics of polymeric (soluble) manganese (IV) oxide (MnO_2) by ferrous iron (Fe^{2+}), Aquat. Geochem. 21 (2015) 143–158.
[13] T. Gao, Y. Shen, Z. Jia, G. Qiu, F. Liu, Y. Zhang, X. Feng, C. Cai, Interaction mechanisms and kinetics of ferrous ion and hexagonal birnessite in aqueous systems, Geochem. Trans. 16 (2015) 16.
[14] J.E. Villinski, P.A. O'Day, T.L. Corley, M.H. Conklin, In situ spectroscopic and solution analyses of the reductive dissolution of MnO_2 by Fe(II), Environ. Sci. Technol. 35 (2001) 1157–1163.
[15] M.A. Hinkle, K.G. Dye, J.G. Catalano, Impact of Mn(II)-manganese oxide reactions on Ni and Zn speciation, Environ. Sci. Technol. 51 (2017) 3187–3196.
[16] C.M. van Genuchten, J. Peña, Sorption selectivity of birnessite particle edges: a d-PDF analysis of Cd(II) and Pb(II) sorption by δ-MnO_2 and ferrihydrite, Environ. Sci. Proc. Impacts 18 (2016) 1030–1041.
[17] Y. Wang, X. Feng, M. Villalobos, W. Tan, F. Liu, Sorption behavior of heavy metals on birnessite: relationship with its Mn average oxidation state and implications for types of sorption sites, Chem. Geol. 292 (2012) 25–34.
[18] L.E. Wasylenki, J.W. Swihart, S.J. Romaniello, Cadmium isotope fractionation during adsorption to Mn oxyhydroxide at low and high ionic strength, Geochim. Cosmochim. Acta 140 (2014) 212–226.
[19] S.R. Randall, D.M. Sherman, K.V. Ragnarsdottir, An extended X-ray absorption fine structure spectroscopy investigation of cadmium sorption on cryptomelane (KMn_8O_{16}), Chem. Geol. 151 (1998) 95–106.
[20] H. Zhao, M. Zhu, W. Li, E.J. Elzinga, M. Villalobos, F. Liu, J. Zhang, X. Feng, D.L. Sparks, Redox reactions between Mn(II) and hexagonal birnessite change its layer symmetry, Environ. Sci. Technol. 50 (2016) 1750–1758.
[21] Q. Wang, P. Yang, M. Zhu, Structural transformation of birnessite by fulvic acid under anoxic conditions, Environ. Sci. Technol. 52 (2018) 1844–1853.
[22] A.A. Simanova, K.D. Kwon, S.E. Bone, J.R. Bargar, K. Refson, G. Sposito, J. Peña, Probing the sorption reactivity of the edge surfaces in birnessite nanoparticles using nickel (II), Geochim. Cosmochim. Acta 164 (2015) 191–204.
[23] Q. Sun, C. Liu, M.E. Alves, S.T. Ata-Ul-Karim, D.M. Zhou, J.Z. He, P.X. Cui, Y.J. Wang, The oxidation and sorption mechanism of Sb on δ-MnO_2, Chem. Eng. J. 342 (2018) 429–437.
[24] B.N.M. Ravel, M. Newville, Data analysis for X-ray absorption spectroscopy using IFEFFIT, J. Synchrotron Radiat. 12 (2005) 537–541.
[25] D. Postma, C.A.J. Appelo, Reduction of Mn-oxides by ferrous iron in a flow system: column experiment and reactive transport modeling, Geochim. Cosmochim. Acta 64 (2000) 1237–1247.
[26] J.P. Lefkowitz, A.A. Rouff, E.J. Elzinga, Influence of pH on the reductive transformation of birnessite by aqueous Mn(II), Environ. Sci. Technol. 47 (2013) 10364–10371.
[27] J. Antelo, M. Avena, S. Fiol, R. López, F. Arce, Effects of pH and ionic strength on the adsorption of phosphate and arsenate at the goethite-water interface, J. Colloid Interface Sci. 285 (2005) 476–486.
[28] M. Kosmulski, pH-dependent surface charging and points of zero charge III. Update, J. Colloid Interface Sci. 275 (2004) 730–741.
[29] M. Villalobos, I.N. Escobar-Quiroz, C. Salazar-Camacho, The influence of particle size and structure on the sorption and oxidation behavior of birnessite: I. Adsorption of As(V) and oxidation of As(III), Geochim. Cosmochim. Acta 125 (2014) 564–581.

[30] Y. Wu, W. Li, D.L. Sparks, The effects of iron(II) on the kinetics of arsenic oxidation and sorption on manganese oxides, J. Colloid Interface Sci. 457 (2015) 319–328.
[31] S. Grangeon, B. Lanson, N. Miyata, Y. Tani, Alain Manceau, Structure of nanocrystalline phyllomanganates produced by freshwater fungi, Am. Mineral. 95 (2010) 1608–1616.
[32] J.E. Johnson, P. Savalia, R. Davis, B.D. Kocar, S.M. Webb, K.H. Nealson, W.W. Fischer, Real-time manganese phase dynamics during biological and abiotic manganese oxide reduction, Environ. Sci. Technol. 50 (2016) 4248–4258.
[33] P. Zhang, W. Yao, S. Yuan, Citrate-enhanced release of arsenic during pyrite oxidation at circumneutral conditions, Water Res. 109 (2016) 245–252.
[34] A.L. Atkins, S. Shaw, C.L. Peacock, Nucleation and growth of todorokite from birnessite: implications for trace-metal cycling in marine sediments, Geochim. Cosmochim. Acta 144 (2014) 109–125.
[35] E.J. Elzinga, Reductive transformation of birnessite by aqueous Mn(II), Environ. Sci. Technol. 45 (2011) 6366–6372.
[36] M. Descostes, F. Mercier, N. Thromat, C. Beaucaire, M. Gautier-Soyer, Use of XPS in the determination of chemical environment and oxidation state of iron and sulfur samples: constitution of a data basis in binding energies for Fe and S reference compounds and applications to the evidence of surface species of an oxidized pyr, Appl. Surf. Sci. 165 (2000) 288–302.
[37] X.Q. Liu, S.H. Li, M.T. Sun, C.L. Yu, B.C. Huang, Preparation, characterization and low-temperature NH3-SCR activity of MnOx/SAPO-11 catalysts, Acta Phys. Chim. Sin. 32 (2016) 1236–1246.
[38] L. Luo, C. Ma, Y. Ma, S. Zhang, J. Lv, M. Cui, New insights into the sorption mechanism of cadmium on red mud, Environ. Pollut. 159 (2011) 1108–1113.
[39] M. Gräfe, B. Singh, M. Balasubramanian, Surface speciation of Cd(II) and Pb(II) on kaolinite by XAFS spectroscopy, J. Colloid Interface Sci. 315 (2007) 21.
[40] B. Lanson, V.A. Drits, E. Silvester, Alain Manceau, Structure of H-exchanged hexagonal birnessite and its mechanism of formation from Na-rich monoclinic buserite at low pH, Am. Mineral. 85 (2000) 826–838.
[41] L. Bochatay, P. Persson, S. Sjöberg, Metal ion coordination at the water-manganite (γ-MnOOH) interface, J. Colloid Interface Sci. 229 (2000) 584–592.
[42] K.D. Kwon, K. Refson, G. Sposito, Surface complexation of Pb(II) by hexagonal birnessite nanoparticles, Geochim. Cosmochim. Acta 74 (2010) 6731–6740.
[43] G. Pan, Y. Qin, X. Li, T. Hu, Z. Wu, Y. Xie, EXAFS studies on adsorption-desorption reversibility at manganese oxides-water interfaces. I. Irreversible adsorption of zinc onto manganite (gamma-MnOOH), J. Colloid Interface Sci. 271 (2004) 28–34.